Spiral wave elimination in memristive neuronal networks under dynamic learning modulated magnetic stimulation

Hong He(贺红), Qian-ming Ding(丁钱铭), Wei-fang Huang(黄卫芳), Ying Xie(谢盈), Ya Jia(贾亚), and Li-jian Yang(杨利建)†

Department of Physics, Central China Normal University, Wuhan 430079, China

Abnormal spiral wave discharges frequently occur in neocortical neural networks, and there is an urgent need for low-intensity, precise intervention to suppress spiking instability. Existing regulatory approaches struggle to keep pace with the dynamic evolution of neural electrical activity, and there is a lack of effective adaptive control methods. This paper puts forward an adaptive magnetic stimulation regulation strategy based on dynamic learning of synchronization (DLS). It can effectively suppress spiral waves via dynamic adjustment of electromagnetic induction strength in memristor Hodgkin-Huxley neuronal networks. We compared three control modes: uniform magnetic stimulation (UMS), alternating magnetic stimulation (AMS), and dynamic learning modulated magnetic stimulation (DLMMS). The results indicate that: the DLMMS can achieve global synchronization of the network at electromagnetic induction strength far lower than that required by the other two modes. Furthermore, its control performance is closely correlated with spatial resolution and learning rate. This finding may provide a new theoretical basis and implementation pathway for the potential application of intelligent optimization algorithms in the development of low-intensity, highly efficient methods for eliminating spiral waves.

Keywords: Dynamic learning of synchronization; Electromagnetic induction; Spiral wave control; Memristive neuronal network.

PACS:

05.45.-a (Nonlinear dynamics and chaos)

87.19.lj (Neuronal network dynamics)

1. Introduction

Spiral waves are self-organized spatiotemporal patterns in nonlinear excitable media, governed by reaction-diffusion equations[1,2]. These vsortex-like rotating waves are widely observed in natural and biological systems, such as the Belousov-Zhabotinsky chemical reaction[3–6]and excitable media including cardiac and neuronal tissues[7,8]. In biological systems, spiral waves often indicate abnormal

† Corresponding author. E-mail: janeyang@ccnu.edu.cn

electrical activity[9], e.g., tachycardia and ventricular fibrillation in the heart[10], as well as epileptic seizures[11,12], Parkinson's disease[13,14] in the cerebral cortex. Therefore, effective and minimally invasive elimination or control of spiral waves is a key interdisciplinary issue in nonlinear dynamics and biomedicine.

Using voltage-sensitive dye imaging techniques, researchers observed stable rotating spiral waves in rat neocortical slices[15]. Their presence is associated with cortical activity, significantly altering EEG oscillation frequency, amplitude, and spatial coherence[16], which suggests that spiral waves in biological media may be modulated by magnetic flux. Transcranial magnetic stimulation (TMS), a non-invasive neuromodulation technique[17–19], generates transient magnetic fields that induce currents in the brain, modulating local neuronal activity[20] while avoiding the discomfort associated with electrical stimulation[21,22]. However, traditional TMS often uses uniform magnetic field or alternating magnetic field[23,24], which cannot dynamically adjust to brain state, leading to limited efficiency and large individual differences[25].

Electromagnetic induction is a key factor affecting neuronal activity[26–30] and describing the mechanisms by which membrane potentials are modulated in the presence of a magnetic field has become a crucial issue. Memristors, as nonlinear resistors with memory[31], couple membrane potential with magnetic flux[32–34], generating complex responses in neuronal systems[35,36]. Memristive neurons (such as memristive FitzHugh-Nagumo model[34]) sense and respond to external electromagnetic fields. Networks of such neurons are called memristive neural networks[32,37–39]. Related theoretical work includes analysis of cardiac tissue under induction[40], energy efficiency improvement in Chay neurons[41], and magnetic field effects on multilayer media[42,43]. In this case, the constructed memristive Hodgkin-Huxley neuron model can reasonably capture the modulatory effect of magnetic stimulation on neuronal electrical activity[44,45]], thus the transmembrane magnetic flux and electromagnetic effects[35,46]are taken into account, providing an ideal model for studying spiral wave control.

The key to eliminating spiral waves is achieving global synchronization, which affects information processing and energy transfer in neural networks[47,48]. Traditional methods adjust topology, periodic driving, or coupling strength, but often rely on prior experience and lack adaptability[49]. Inspired by the concept of dynamic learning in the training of artificial neural networks, researchers have proposed the dynamic learning of synchronization (DLS) method[46–48,50,51] based on recursive least squares. By capturing state differences between nodes in real time, this method adaptively adjusts control parameters, such as coupling strength or external stimulation[52]. A great deal of work has already been carried out in this field: low-intensity adaptive electric shock for cardiac spiral waves[53], DLS-based unpinning and elimination of spiral waves[54], dynamic learning-optimized photon scanning[55]. The DLS method responds to system changes in real time with good robustness and generalization.

Although some progress has been made in previous research into the elimination of spiral waves in the cerebral cortex via magnetic fields[53–58], there has been a lack of

in-depth investigation into adaptive magnetic stimulation modulation in mammalian neocortex. The memristive Hodgkin–Huxley (mHH) model is capable of characterizing the coupling dynamics between electromagnetic fields and neurons, and simulating cortical neural activities under magnetic stimulation. In this paper, an adaptive magnetic stimulation strategy is constructed based on dynamic learning to investigate the elimination of spiral waves within such neural networks. We discussed several forms of magnetic stimulation, including uniform magnetic stimulation (UMS) and alternating magnetic stimulation (AMS), as well as dynamic learning modulated magnetic stimulation (DLMMS). The results show that DLMMS can efficiently eliminate spiral waves in a shorter time and at a significantly lower electromagnetic induction intensity.

The remainder of the paper is organized as follows. The memristive neural network is introduced in Section 2.1, the magnetic induction currents and the principles of DLS adaptive control are elaborated in Section 2.2, and the statistical measures are presented in Section 2.3. The control of spiral waves via UMS is examined in Section 3.1, and spiral wave regulation through AMS is analyzed in Section 3.2. The effectiveness of DLMMS in spiral wave control is explored in Section 3.3. Finally, the electromagnetic induction intensity and convergence times required for global synchronization realization with the three aforementioned methods are compared. The physical mechanisms and potential applications of adaptive magnetic stimulation are discussed, and overall conclusions are summarized in Section 4.

2. Model and methods

单击此处输入文字。

2.1. Neuronal network model

In this paper, given that an external changing magnetic stimulation induces currents in neocortex excitable media, a memristor is introduced to describe the Hodgkin–Huxley model. We construct a 120×120 Hodgkin-Huxley-type network with no-flux boundary conditions. In the spiral wave, the improved HH model considering electromagnetic induction is adopted to describe the dynamic activity of neurons. By introducing a magnetic flux into the neurons and employing a memristor to characterize the coupling between membrane potential and magnetic flux, the expression of the mHH model[32,42] considering electromagnetic induction is as follows:

$$\begin{cases} C\dfrac{\partial \mathrm{u}}{\partial t} = D\nabla^2 u + f(u) + I_{\varphi}, \\ f(u) = I_K + I_{Na} + I_L + I_{ext}, \\ \dfrac{dy}{dt} = \dfrac{1}{\tau_y}\left(-y + y_{\infty}\right), \quad (y = n, m, h). \end{cases} \tag{1}$$

In Eq.(1), u represents the membrane potential of individual neurons, C is the membrane capacitance taking the value of 0.75 μF/cm^2. The diffusion term $D\nabla^2 u$ describes the spatial electrical coupling of the membrane potential, where D = 1.865

mS/cm^2 denotes diffusion coefficient, and ∇^2 is Laplacian operator. The diffusion term can be discretized as follows[59]:

$$D\nabla^2 u = \frac{D}{6}[4(u_{i-1,j}+u_{i+1,j}+u_{i,j-1}+u_{i,j+1})+(u_{i-1,j-1}+u_{i+1,j+1}+u_{i+1,j-1}+u_{i-1,j+1})-20u_{i,j}], \tag{2}$$

where the discretization results imply that each node (i, j) is connected to the other eight nodes in its vicinity: namely the four nearest neighbours and the four next-nearest neighbours.

I_K, I_{Na}, I_{L} are the sodium, potassium and leaky ion currents received by neurons, respectively, with their specific expressions as follows:

$$\begin{cases} I_K = g_K n(u_K - u), \\ I_{Na} = g_{Na} m^3 h(u_{Na} - u), \\ I_L = g_L(u_L - u), \end{cases} \tag{3}$$

where g_{K} = 40 mS/cm^2, g_{Na} = 150 mS/cm^2, g_{L} = 0.033 mS/cm^2 represent the maximum conductivities of potassium ions, sodium ions and leakage ions, respectively. u_{K} =−90mV, u_{Na} = 60mV, u_{L} = −70mV represent the reversal potentials of potassium ions[60], sodium ions and leakage ions, respectively. The external forcing current I_{ext} is set to 1.5μA/cm^2 in all nodes.

In Eq.(1), n, m and h are gating parameters of the ion channel, with values ranging from 0 to 1. τ_y and y_∞ satisfy equations of the following form:

$$\begin{cases} \tau_n = \dfrac{1}{\alpha_n+\beta_n}, \quad n_\infty = \dfrac{\alpha_n}{\alpha_n+\beta_n}, \\ \tau_m = \dfrac{1}{\alpha_m+\beta_m}, \quad m_\infty = \dfrac{\alpha_m}{\alpha_m+\beta_m}, \\ \tau_h = \dfrac{1}{\alpha_h+\beta_h}, \quad h_\infty = \dfrac{1}{1+e^{(u+60)/6.2}}, \end{cases} \tag{4}$$

and the conversion rates of the ion channels are as follows:

$$\begin{cases} \alpha_n = \dfrac{0.01(u-30)}{1-\exp[-(u-30)/9]}, \quad \beta_n = -\dfrac{0.002(u-30)}{1-\exp[-(u+30)/9]}, \\ \alpha_m = \dfrac{0.182(u+30)}{1-\exp[-(u+30)/8]}, \quad \beta_m = -\dfrac{0.124(u+30)}{1-\exp[-(u+30)/8]}, \\ \alpha_h = \dfrac{0.028(u+45)}{1-\exp[-(u+45)/6]}, \quad \beta_h = -\dfrac{0.0091(u+70)}{1-\exp[-(u+70)/6]}. \end{cases} \tag{5}$$

In Section 2.2, we shall continue our study of the magnetic induced current I_φ arising from changes in magnetic flux and magnetic field.

2.2. The electromagnetic induction current

To reproduce the electromagnetic induction effect in a neuronal model, we introduce the magnetic flux φ here, and the memristor mediates the coupling between

the membrane potential and the magnetic flux[34]. As shown in Fig. 1, by regulating the electromagnetic induction intensity, a magnetic induction-induced current I_{φ} can be induced in excitable medium. This current modulates the neuronal membrane potential and ultimately achieves control of spiral waves.

In the mHH model, the induced current resulting from magnetic stimulation is denoted as I_{φ} and is expressed as follows:

$$I_{\varphi} = -k(\alpha + 3\beta\varphi^2)u, \tag{6}$$

where k is the electromagnetic induction strength, and φ is the magnetic flux passing through the neuron. $\alpha+3\beta\varphi^2$ is the memductance of the memristor controlled by the magnetic flux, which describes the coupling between the magnetic flux and the neuronal membrane potential. The term $k(\alpha+3\beta\varphi^2)$ describes the inhibition modulation of membrane potential. In this context, $\alpha = 0.4$ and $\beta = 0.02$[35,60] as fixed parameters, and φ satisfies the following expression:

$$\frac{d\varphi}{dt} = k_1 u - k_2\varphi + A\sin(2\pi\omega t), \tag{7}$$

where k_1u and $k_2\varphi$ respectively reflect the influence of membrane potential on magnetic flux and magnetic leakage, and the parameters of the electromagnetic effect are $k_1 = 0.001$and $k_2 = 0.01$. $A\sin(2\pi\omega t)$ represents the effect of external electromagnetic induction on node, and A and ω denote the amplitude and frequency, respectively. Based on the temporal evolution characteristics of magnetic stimulation, three magnetic stimulation modes are investigated in this paper.

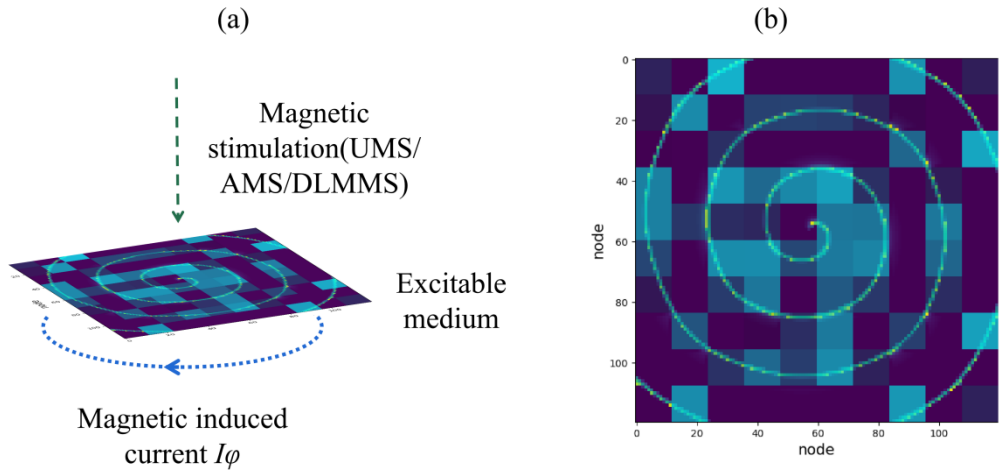


Fig. 1 Schematic diagram of adaptive magnetic flux control. (a) Schematic illustration of the generation of induced current by magnetic stimulation in an excitable medium. The central panel depicts a neuronal network within excitable medium. An external magnetic stimulus (green dotted line) is applied; this stimulus penetrates the medium and induces an induced current (blue dotted line). (b) A snapshot of the elimination of spiral waves under the DLMMS; the blue blocks hovering above the spiral wave represents the local electromagnetic induction strength, whilst the brightness of the colored area indicates the spatial distribution of magnetic flux, illustrating the non-uniform regulatory characteristics during the synchronization process of the driving network.

The first mode is the UMS, where the magnetic stimulation remains constant

during the control process, A=0. This method is simple and easy to implement, but lacks the ability to respond to the dynamic changes of the medium, resulting in a relatively high required electromagnetic induction strength. A detailed discussion will be presented in Section 3.1.

The second mode is the AMS, whose intensity exhibits periodic changes over time, expressed. By adjusting the amplitude, A and frequency ω, resonance with the natural frequency of the medium may be induced. See further details in Section 3.2.

The third mode is DLMMS, which is the core method adopted in this paper. In this mode, k is no longer preset, A=0, but is dynamically updated based on the DLS method according to the real-time membrane potential differences of the nodes in the network. Its core idea is to adaptively adjust the intensity by capturing the deviation between the membrane potential of each node and the target membrane potential in real time, thereby guiding the network toward global synchronization with minimal intensity. We aim to regulate the electromagnetic induction strength applied to the excitable medium using the DLS method, thereby achieving synchronization of neuronal firing in the neural network. To apply the DLS method for synchronization control, it is first necessary to obtain the membrane potentials of the target nodes. The membrane potential differences are then used to update the learning parameters, and the training results are subsequently applied directionally to these nodes as a driving force. As the membrane potential fluctuates, the magnetic flux is continuously adjusted, thereby affecting the magnetic induction-induced current. The induced current diminishes to zero only when the target nodes achieve synchronization at which point the spiral waves in excitable medium are eliminated. The membrane potential $u(t)$ obtained from the simulation can be used to calculate the average membrane potential $u_{\mathrm{mean}}(t)$ within each block based on its dynamic characteristics:

$$u_{mean}(t)=\frac{u_{\max}(t)+u_{\min}(t)}{2} \tag{8}$$

where $u_{\max}(t)$ and $u_{\min}(t)$ represent the maximum and minimum values, respectively, of the membrane potential within the block at time t. During this process, the DLMMS adjusts the intensity of the applied magnetic stimulation based on the average membrane potential within each block. If the size of a block is d, then the number of nodes covered by each block is $n = d^2$, and the total number of blocks in the network is N/n.

The externally controllable magnetically induced current I_{φ} is the core subject of the DLMMS. The dynamics function of the control term is $g(u_i) = (\alpha+3\beta\varphi^2)u_i$. The first equation in Eq.(1) is discretized by applying Euler's algorithm, and the following result is obtained:

$$u_i' = u_i + [f(u_i) + D\nabla^2 \mathrm{u}_i + kg(u_i)]\Delta t, \tag{9}$$

where the superscript ' on a variable is used to distinguish between the current value at time t and the updated new value at time $t+\Delta t$, with Δt being the time step. At the same time, Eq.(7) can be written in discrete form as:

$$\varphi' = \varphi + [k_1 \mathrm{u} - k_2\varphi + A\sin(2\pi\omega t)]\Delta t. \tag{10}$$

Next, by splitting Eq.(9) into a system term and a control term, we obtain:

$$\begin{cases} F_i = u_i + \left[f(u_i) + D\nabla^2 \mathrm{u}_i \right] \Delta t, \\ G_i = g(u_i)\Delta t. \end{cases} \tag{11}$$

When spiral waves are eliminated, the nodes in the network become synchronized. After a period of evolution, the medium will gradually approach either a resting state or a state of synchronized firing. At this point, the condition $u_i = u_{\text{mean}}$ among nodes is sufficient to suppress the generation of new spiral waves. The ultimate goal of the G_i term is to minimize the difference between these two quantities:

$$L_i = \arg\min \frac{1}{2} \left\| kG_i - \left[u_{\text{mean}} - F_i \right] \right\|^2, \tag{12}$$

to determine the electromagnetic induction strength k required for optimal synchronization at node i, it is necessary to find the point where the derivative of the loss function is zero:

$$\frac{dL_i}{dk} = G_i \left\{ kG_i - \left[u_{\text{mean}} - F_i \right] \right\} = 0, \tag{13}$$

the analytical solution of k thus obtained is as follows:

$$k = \frac{G_i \left[u_{\text{mean}} - F_i \right]}{\left\| G_i \right\|^2}, \tag{14}$$

at each time step, k is readjusted for the selected nodes until the spiral waves are eliminated. The detailed solution process can be found in our previous work[54]. The core recursive equation of the DLS method is thus obtained as follows:

$$\begin{cases} k' = k - \lambda_i \left(u'_i - u'_{mean} \right), \\ \lambda_i = \dfrac{P_i G'_i}{1 + \left(G'_i \right)^T P_i G'_i}, \\ P'_i = P_i - \lambda_i \left(G'_i \right)^T P_i, \end{cases} \tag{15}$$

where the initial value satisfies $P_i(0) = \alpha I$, with I being the identity matrix. α is the learning rate, whose value reflects the response sensitivity of the DLS method to asynchrony between nodes. A larger value of α leads to a faster growth rate of k, thereby enabling faster synchronization of the nodes. The value can be adjusted according to the requirements under different conditions. Next, we introduce the statistical measurement methods.

2.3. The measurements

Loss of synchronization is the core cause of abnormal dynamic behaviors in excitable media. Electrical synchronization is a key prerequisite for maintaining the macroscopic ordered dynamics of the medium. Once synchronization is disrupted, the medium becomes prone to the formation of non-uniform patterns such as spiral waves, which may further evolve into spatiotemporal turbulence, leading to dynamic

instability of the system. Here, we introduce the synchronization factor R as a core indicator for quantitatively characterizing the degree of synchronization in the medium, with its expression given as follows:

$$\begin{cases} F = \dfrac{1}{N}\sum_{i=1}^{N} u_i, \\ R = \dfrac{\left\langle F^2 \right\rangle - \left\langle F \right\rangle^2}{\dfrac{1}{N}\sum_{i=1}^{N}\left(\left\langle u_i^2 \right\rangle - \left\langle u_i \right\rangle^2\right)}, \end{cases} \tag{16}$$

where u_i denotes the membrane potential of the i-th node in the network, the symbol $\langle\ \rangle$ represents the time-averaged value over the statistical period, N is the total number of nodes (in the simulation, N = 120×120 = 14,400) and F is the average membrane potential of the nodes, reflecting the overall electrical activity level of the medium. The value of the synchronization factor R exhibits a clear correspondence with the dynamic state of the medium: when R approaches 1, the electrical activity of the nodes in the medium is highly synchronized, and the system is in an ordered steady state; when R approaches 0, the phase coherence of the nodal electrical activity is disrupted, and the system exhibits dynamically unstable states such as spiral waves and turbulence.

To quantitatively describe the magnitude of electromagnetic induction strength in the DLS method, we define the average k, denoted as k_{mean}, with its equation given as follows:

$$k_{mean} = \left\langle \frac{1}{N}\sum_{i=1}^{N} \left|k_i\right| \right\rangle, \tag{17}$$

where N is the total number of nodes in the network, and k_i is the electromagnetic induction strength at node i. This metric is used to evaluate the level of electromagnetic feedback strength required to achieve global synchronization under different control modes.

In order to comprehensively evaluate the actual driving effects of different control modes on the synchronization rate, it is necessary to quantitatively characterize the time evolution of the system's state as it approaches synchronization; the convergence time τ_c is therefore defined as follows:

$$\tau_c = t - t_{sync}, \tag{18}$$

where t represents the duration of the simulation run, whilst t_{sync} denotes the time at which the network is in a state of global synchronization. τ_c is used to quantitatively measure the speed at which the network achieves consistency under different control modes. A smaller value of τ_c indicates that the corresponding electromagnetic induction strength is more effective in promoting synchronization; conversely, a larger value suggests that the synchronization efficiency of that control mode is lower.

3. Results

In this paper, the reaction-diffusion system is numerically integrated using the forward Euler method, and all simulations are performed in the Python environment. In the computation, the two-dimensional grid consisting of 120×120 nodes are reshaped into a one-dimensional column vector containing 14,400 nodes and multiplied by the Laplacian matrix to discretize the diffusion coupling term. The simulation time step is set to $\Delta t = 0.1$ms.

3.1. Uniform magnetic stimulation

This section aims to investigate the regulatory effect of uniform magnetic stimulation on spiral waves. The simulation procedure is as follows: First, stable spiral waves are induced in the network under specific initial conditions. Subsequently, a uniform electromagnetic induction strength k is applied for a duration of 100 ms, during which the evolution behavior of the spiral waves and the global synchronization state of the network are observed in real time. To further quantify the control effectiveness under different electromagnetic induction strength, we introduce the synchronization factor R to analyze the network waveforms for various values of k, thereby delineating the parameter interval within which effective regulation can be achieved.

First, we discuss the waveform evolution under uniform electromagnetic induction strength over a period of time and observe the changes of spiral waves in the network.

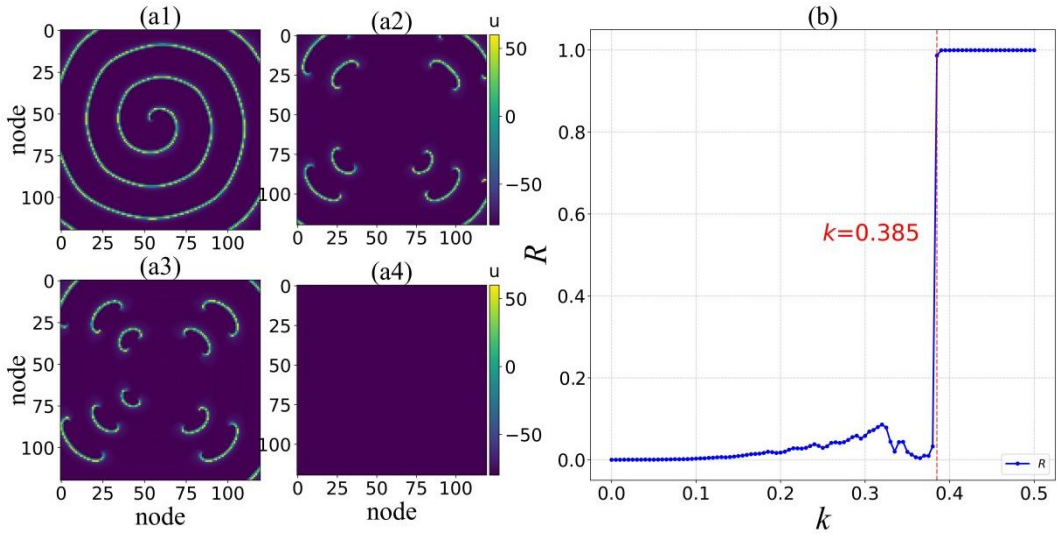


Fig. 2 Elimination of spiral waves under uniform electromagnetic induction strength and the corresponding synchronization statistics. As the density increases, the spiral waves are gradually eliminated, and the network eventually enters a fully synchronized state. The threshold strength is $k = 0.385$. (a1)-(a4) show snapshots of the spatial distribution of the membrane potential at $t = 100$ ms for $k = 0.25$, 0.30, 0.35 and 0.40. As k increases, the spiral wave packets disintegrate and drift, and the system transitions from an ordered spiral wave state through a disordered state to a synchronized state. (b) The behaviour of the synchronization factor R as a function of k shows that when $k > 0.385$, the system undergoes a sudden transition from a non-synchronous spiral wave state to a fully synchronized resting state, which is consistent with the phenomenon observed in (a4).

Further simulations indicate that the dynamics of a spiral wave are essentially determined by the dynamics of its core region—the spiral seed. When k exceeds the critical value ($k > 0.385$), the network achieves complete synchronization, indicating that the spiral waves are completely eliminated under the action of the UMS. We examined the system evolution process under different feedback strength, setting k = 0.25, 0.30, 0.35**,** 0.40 [Figs. 2 (a1)-(a4)]. Under a low feedback strength, the spiral seed maintains a stable rotating rhythm, and the spiral wave structure remains intact without being eliminated [Fig. 2(a1)]. As the feedback strength increases to a moderate level [Figs. 2(a2)-(a3)], the spiral seed gradually becomes unstable, the wavefront breaks up, and a turbulent state is induced in the network. When the feedback strength further increases and exceeds the critical threshold ($k > 0.385$), the spiral seed is completely destroyed, the spiral waves disappear, and the network enters a globally synchronized resting state [Fig. 2(a4)].

The statistical relationship between network synchronization and the strength k is shown in Fig. 2(b). The results indicate that as the strength k increases, the synchronization factor R exhibits an overall upward trend. It is worth noting, however, that this increase is not a simple linear accumulation but exhibits a distinct nonlinear jump around $k \approx 0.385$: the synchronization factor rapidly jumps from a low value to nearly 1.0 [Fig. 2(b)]. This jump phenomenon reveals that the suppressive effect of magnetic stimulation on spiral waves exhibits a typical threshold effect the spiral wave becomes unstable and eventually annihilates only when the applied electromagnetic induction strength is sufficient to disrupt the self-sustained rhythm of the spiral seed. Once this critical point is exceeded, the system enters a globally synchronized state. Beyond this threshold, further increasing the strength k leaves the network in a globally synchronized state under the UMS.

3.2. Alternating magnetic stimulation

In this section, we investigate the effects of an external magnetic stimulation with periodic magnetic flux variation on the neuronal network, with amplitude A and frequency ω. The simulation procedure in this section is consistent with that in Section 3.1. Finally, the synchronization factor is used to statistically analyze the synchronization changes of the neuronal network under the non-uniform periodic external magnetic flux with varying amplitude A and frequency ω .

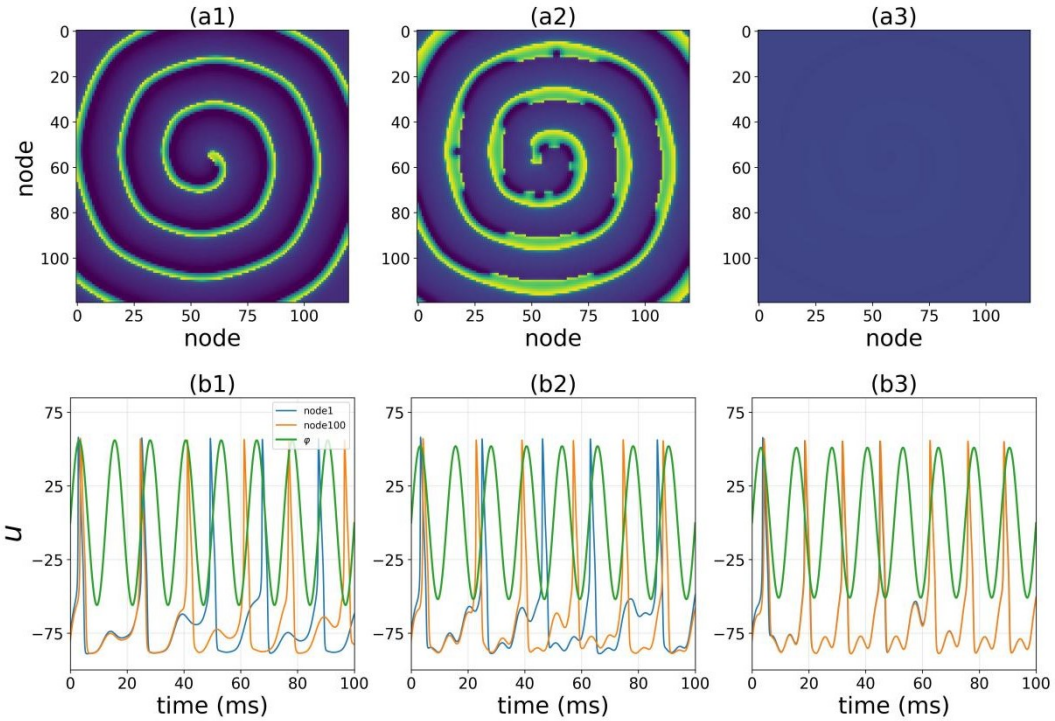


Fig. 3 The effect of the amplitude of AMS on the spatiotemporal dynamical behaviour of a network. Fixed parameters: k = 0.045, ω = 0.0008kHz. (a1)-(a3) show snapshots of the spatial distribution of the membrane potential at t = 100 ms for different amplitudes A = 2.0, 4.0, 6.0. (b1)-(b3) show the membrane potential time series at nodes (1, 1) and (100, 100) for the corresponding amplitudes, illustrating how the nodes change as k and t vary. As A increases, the network map undergoes significant changes, indicating that AMS have a marked modulatory effect on neuronal electrical activity.

In Fig. 3, we can clearly observe that after introducing the periodic external magnetic flux, as the amplitude A of the periodic magnetic stimulation increases, the spatiotemporal patterns of the network exhibit significant changes. When A =2.0 [Figs. 3(a1) and Figs.(b1)], the spiral wave structure remains essentially stable, and the node membrane potentials exhibit periodic oscillations. When A increases to 4.0 [Figs. 3(a2) and Figs.(b2)], the spiral wave tip begins to destabilize, the wavefront undergoes fragmentation, and a turbulent state emerges in the network, accompanied by a decrease in the synchronization of the node membrane potential time series. When A further increases to 6.0 [Fig. 3(a3) and Figs.(b3)], the synchronization of the node membrane potential time series becomes increasingly higher until the spiral waves in the network are eliminated, and the network enters a globally synchronized resting state.

The above results indicate that the amplitude of the periodic external magnetic stimulation exerts a significant modulatory effect on the evolution of spiral waves. However, amplitude is not the only factor determining the effectiveness of magnetic stimulation regulation; the frequency of the magnetic stimulation is also a key parameter affecting the dynamic behavior of spiral waves. To investigate the role of the frequency of the periodic external magnetic stimulation in the process of spiral wave elimination, we further examined the effects of periodic magnetic stimulation

with different frequencies on the spatiotemporal dynamics of the network under fixed amplitude and electromagnetic induction strength. The results are shown in Fig.4.

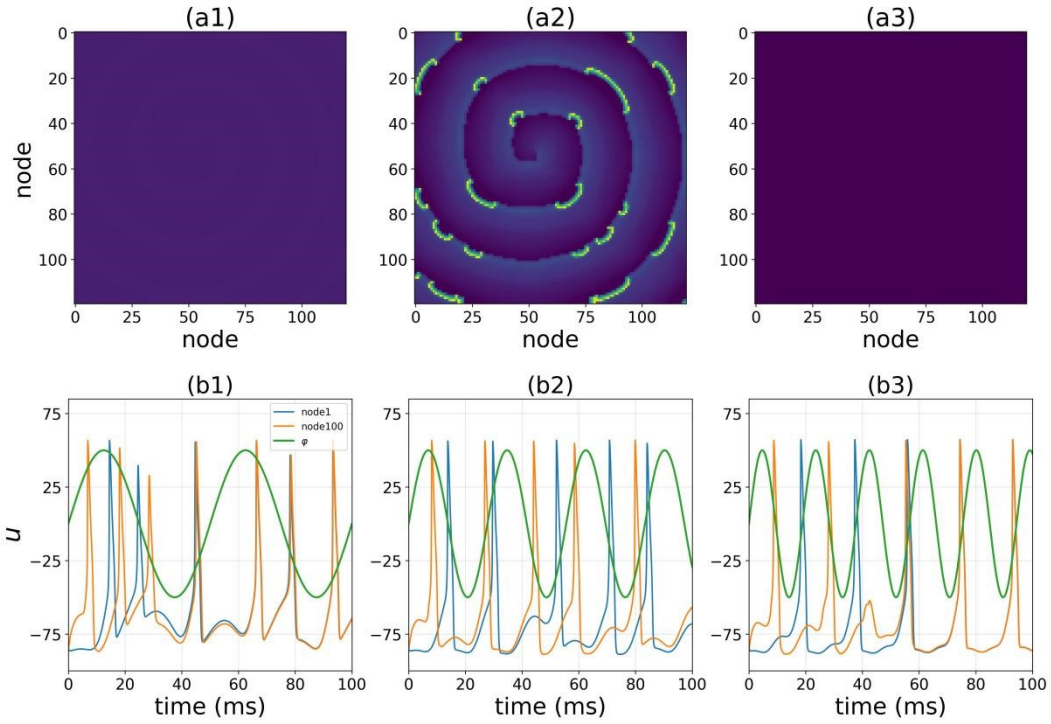


Fig. 4 Modulation of the spatiotemporal dynamics of the network by the frequency of AMS. Fixed parameters: A = 2.0 and k = 0.045. (a1)-(a3) show snapshots of the spatial distribution of the membrane potential at different frequencies ω=0.0002kHz, 0.00036kHz, 0.00053kHz. (b1)-(b3) show the membrane potential time series for network nodes (1, 1) and (100, 100) at the corresponding frequencies, illustrating those different frequencies of AMS elicit different response characteristics in spiral waves.

From the figure, it can be observed that as the frequency ω increases, the spatiotemporal patterns of the network exhibit non-monotonic evolution characteristics. When the frequency is low ω =0.0002kHz [Figs. 4(a1) and Figs.(b1)], the frequency matches the intrinsic dynamics of the spiral wave tip, effectively disrupting its self-sustained rhythm. The spiral waves are largely eliminated, and the network tends toward synchronization. As the frequency increases to ω =0.00036kHz [Figs. 4(a2) and Figs.(b2)], the frequency deviates from the resonance range. The spiral wave tip begins to destabilize but is not yet eliminated, and the synchronization of the node membrane potential time series decreases. When the frequency further increases to ω =0.00053kHz [Figs. 4(a3) and Figs.(b3)], the frequency becomes higher and re-enters the resonance range, achieving synchronization.

These results indicate that the frequency of the external magnetic stimulation is a key parameter in regulating the dynamics of spiral waves. Similar to the effect of amplitude, there exists a resonant frequency for spiral wave elimination-only when the frequency of the external periodic magnetic stimulation matches the intrinsic rhythm of the spiral wave tip (or is sufficient to disrupt it) can the self-sustained oscillation of the spiral seed be effectively broken, achieving globally synchronized control of the network.

Fig.5 further reveals, from a two-dimensional parameter space, the synergistic regulatory mechanism of the amplitude A and frequency ω of a periodic external magnetic stimulation on the network's synchronous state. Under a fixed strength of k = 0.045, we investigated the synchronization response characteristics of the network for various combinations of amplitude A and frequency ω. Fig.5 shows the two-dimensional statistical results of the synchronization factor R as a function of frequency ω and amplitude A.

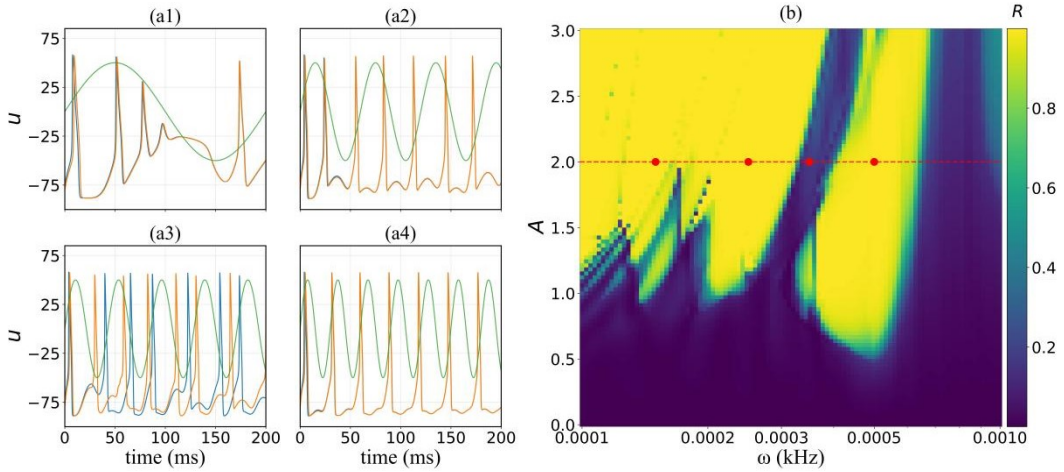


Fig. 5 Synergistic regulation of network synchronization states by the amplitude and frequency of AMS. Fixed parameters: k = 0.045. (a1)-(a4) show the membrane potential sequences at nodes (1, 1) and (100, 100) for, under the influence of ω = 0.00015kHz, ω = 0.00025kHz, ω = 0.00035kHz, and ω = 0.0005kHz at different frequencies. (b) The figure shows the two-dimensional statistical results of the synchronization factor R as a function of frequency ω and amplitude A. The four red solid points on the dashed line correspond to the states shown in Figs. (a1)-(a4), respectively.

Figs. 5(a1)-(a4) shows the time series of node membrane potentials at different frequencies under a fixed amplitude of A=2.0. To facilitate the observation of the membrane potential sequences reflecting the network's synchronous state, we extended the simulation time to 200 ms (increasing the simulation time does not affect the simulation results; The simulation duration in the statistical graph remains at 100 ms). This provides clear evidence of the aforementioned parametric relationship: when ω = 0.00015kHz [Fig. 5(a1)] and ω = 0.00025kHz [Fig. 5(a2)], the system is in a synchronized state, and the membrane potential sequences of the two nodes are highly consistent; When ω increases to 0.00035kHz [Fig. 5(a3)], the system deviates from the optimal synchronization window, and a marked difference appears in the membrane potential sequences of the two nodes; the network is in an asynchronous state; When ω is further increased to 0.0005kHz [Fig. 5(a4)], the system re-enters synchronization, and the membrane potentials at the two nodes once again converge.

Further examination of the two-dimensional phase diagram reveals that the network's synchronization state exhibits a multi-region distribution in parameter space, with two main synchronization control regions: One is the low-frequency, high-amplitude region (A > 1.0, 0.0001kHz < ω < 0.00032kHz), in which the synchronization factor R also approaches 1, indicating that extremely low-frequency

magnetic stimulation can still effectively cancel out spiral waves and achieve network synchronization when the amplitude is sufficiently large; Another is the mid-frequency region (A > 1.0, 0.00039kHz < ω <0.00065kHz), which is another highly efficient synchronization control window. However, as the frequency increases further (ω>0.00065kHz), the magnetic stimulation changes too rapidly to effectively influence the slow-varying dynamics of the spiral waves; consequently, the synchronization factor drops significantly, and the network struggles to achieve full synchronization.

Taking the above results together, it can be concluded that alternating magnetic stimulation utilizes the resonance effect between its frequency and the intrinsic rhythm of the helical wavefront; within the resonance band, it can effectively eliminate the helical waves and achieve global synchronization. This method offers advantages such as low force requirements, multiple effective control windows and flexible adjustment; however, its damping effectiveness is highly dependent on frequency resonance and requires precise coordination with amplitude, making parameter matching rather demanding.

3.3. Dynamic learning modulated magnetic stimulation

The electrical activity of neural networks is significantly modulated by electromagnetic induction. To effectively suppress abnormal discharge modes such as spiral waves in the network, this paper introduces the DLS method to achieve adaptive control of the value of k. This section will systematically explain the fundamental principles of the DLS method for modulating magnetic flux in excitable media, as well as its specific applications in spiral wave control.

The DLS method is an adaptive control algorithm based on recursive least squares; its core principle involves dynamically updating control parameters by collecting membrane potential signals from network nodes in real time, thereby driving the network to gradually converge towards a state of global synchronization[41]. This method requires no prior training, offers good real-time performance and adaptability, and is suitable for non-linear systems where the model is uncertain or the environment is changing. In this study, we applied the DLS method to mHH model to achieve adaptive suppression of spiral waves by dynamically adjusting the value of k.

During the simulation, we perform synchronous training on all nodes within the medium. The simulation procedure is set out as follows: first, allow the spiral wave to evolve freely for 5 ms; Next, initiate DLS training; the training lasts for 25 ms; Finally, the training is terminated, and the system is monitored for a further 70 ms to determine whether the network has entered a globally synchronized resting state. Ideally, the control system should be able to adjust the feedback strength in real time based on the global membrane potential of the medium, thereby effectively eliminating the spiral waves.

Figs. 6(a1), (a2) and (a3) illustrate the control performance of spatial spiral waves when the learning rate α =0.001, and the size of the block, which is the spatial resolution of k is 12×12 nodes (denoted as 12-node); we systematically analyze the dynamic adjustment process of the feedback intensity based on the DLS method at

this resolution. Fig.6 illustrates the evolution of the membrane potential, magnetically induced current and feedback strength over time at this resolution, providing an intuitive basis for understanding the dynamic control behaviour of the DLS method in the regulation of helical waves.

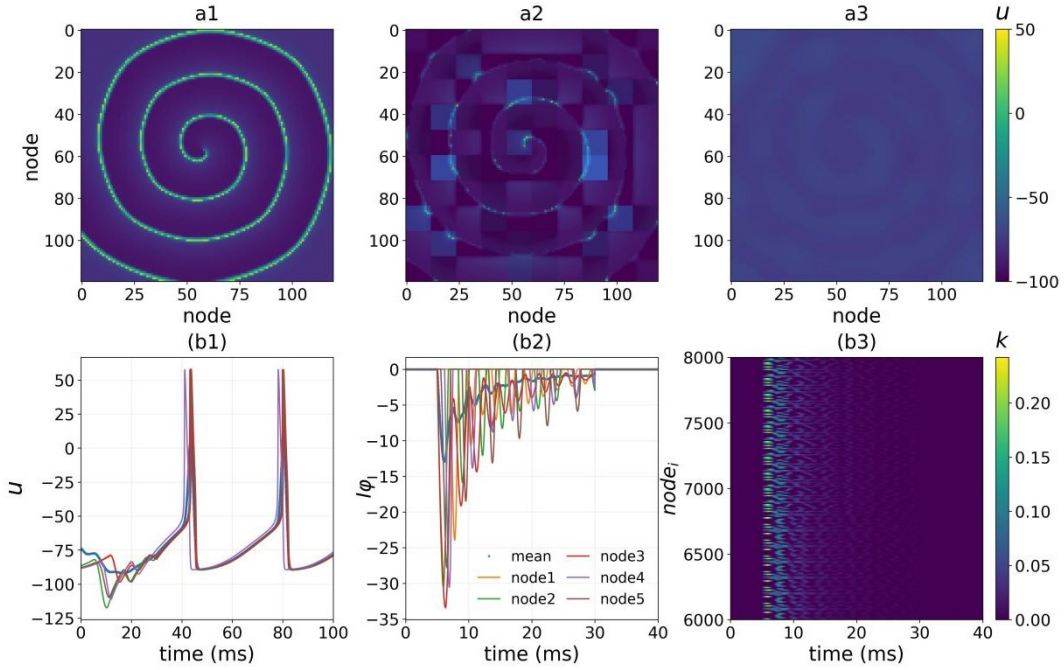


Fig. 6 Elimination of spiral waves based on DLMMS. Fixed parameters: α = 0.0001, resolution is 12-node. (a1), (a2) and (a3) are spatial snapshots at t = 0, 25 ms and 100 ms, respectively. (b1) shows discharge waveforms for the membrane potential at different nodes. (b2) shows the magnetic induction currents at different nodes. (b3) illustrates the evolution of the k-values of some neurons during the dynamic adjustment process. Here, the nodes in the two-dimensional space are sequentially unfolded into a one-dimensional index, where i denotes the node number ($i \in [1, N]$).

The process of eliminating helical waves under the influence of DLMMS is shown in Figs. 6(a1)-(a3). In the simulation, after 5 ms, a value of k controlled by the DLS method is introduced into the network, inducing a decrease in the membrane potential in regions of the medium with high membrane potential (action potential nodes), thereby achieving global synchronization. During this process, the membrane potential of the spiral wave, the magnetically induced current and the variation in the magnetically induced current can be observed in Fig. 6(b1), Fig. 6(b2) and Fig. 6(b3). The results show that, as the network gradually achieved global synchronization, the k-value of each neuron underwent a marked change. During the initial phase of DLMMS operation, as shown in the early part of Fig. 6(b1), it can be seen that the firing state of the neurons in the network is unstable. At the same time, a marked change in the k-value is observed at around 5-15 ms in Fig. 6(b3). Subsequently, the differences in firing patterns among the neurons in the network diminish; at this stage, the value of k changes only slightly, and the network gradually synchronizes; when all nodes are firing in a regular pattern, the value of k for each neuron gradually decreases to 0.

The above discussion highlights a key feature of the DLMMS: there is a close correlation between the regulation of the k value in neurons and their firing activity. This method is capable of accurately identifying differences in firing patterns between neurons and, based on this, dynamically adjusting the feedback strength of each unit, thereby achieving global synchronization of the neural network. However, in practice, control systems are often subject to physical limitations in terms of spatial resolution, which naturally raises a key question: given that it is not possible to regulate each node independently, what level of resolution is required to ensure effective suppression of the spiral wave? To investigate the above issues, we fixed the learning rate α at 0.0001 in Fig. 7 and examined the suppression effect on spiral waves by varying the spatial resolution to 10-node, 12-node, and 15-node.

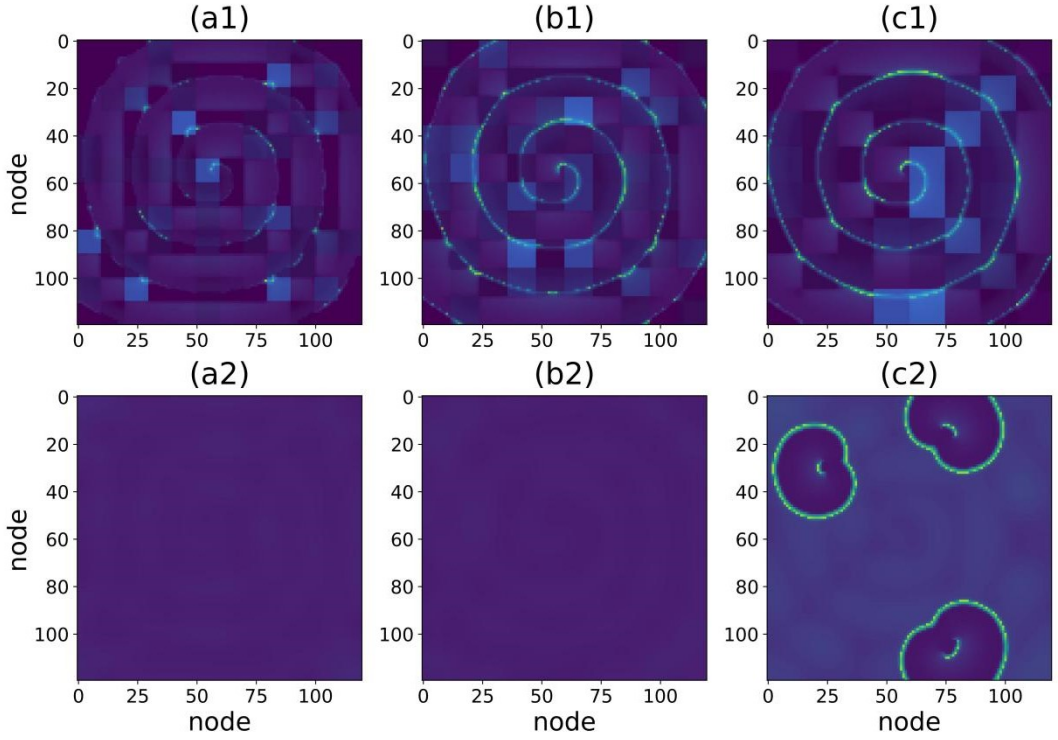


Fig.7 The effectiveness of spiral wave control using the DLMMS at different resolutions. Fixed parameters: α = 0.0001. (a1)-(c1) and (a2)-(c2) show snapshots of the spatial distribution of the membrane potential at 10 ms and 100 ms during the control process, respectively, where (a1)-(a2), (b1)-(b2) and (c1)-(c2) correspond to resolution of 10-node, 12-node and 15-node, respectively (the smaller the node size, the higher the resolution of k). It can be seen that when the resolution is 10-node, the spiral wave is completely eliminated; when the resolution is 12-node, the wavefront breaks up and synchronization is not achieved; when the resolution is 15-node, control fails and the spiral wave continues to rotate.

In Fig. 7(a1), Fig. 7(a2) and Fig. 7(b1), Fig. 7(b2), the spiral waves were successfully suppressed at the 10-node and 12-node resolutions; however, they could not be suppressed at the 15-node resolution, and under this magnetic field strength, the spiral waves exhibited abnormal propagation. This is because the lower resolution is unable to resolve the wave wall (the thickness of the mHH wave wall is approximately 12 nodes), and can only enhance the magnetic induction intensity to force the system into synchronization. As can be clearly seen in Fig. 7(c2), the

left-hand half of the spiral wave that had not yet been eliminated is re-excited, and new spiral wave seeds are induced in the network following the removal of the DLMMS.

The above results indicate that, under a fixed learning rate α, the spatial resolution has a decisive influence on the effectiveness of spiral wave control. The higher the resolution, the more precisely the control system can act on the core region of the spiral wave, resulting in a more significant suppression effect. When the resolution exceeds the scale of the spiral wave's wall, the control capability decreases significantly. It can therefore be inferred that the effectiveness of the DLMMS control strategy is highly dependent on spatial resolution: the higher the resolution, the more precisely the control system can act on the core region of the spiral wave, resulting in a more significant suppression effect; conversely, insufficient resolution makes it difficult to achieve global synchronization. In this 120×120 node network, due to the DLMMS mechanism, the network must be divided into an integer number of square blocks; this means that the length of a block can only take discrete values, whilst the size of a block satisfies $(d_i)_{i=1}^{16}$ ={1,2,3,4,5,6,8,10,12,15,20,24,30,40,60,120}. It therefore follows that the smaller the block size, the higher the corresponding resolution. When the block size exceeds 24-node, the network operates entirely in an asynchronous state; we shall therefore not consider such cases. To illustrate this more clearly, we have compiled statistics on the network's R and k values for different block sizes and learning rates. (In the simulation, R and k are still calculated based on 120×120 nodes.)

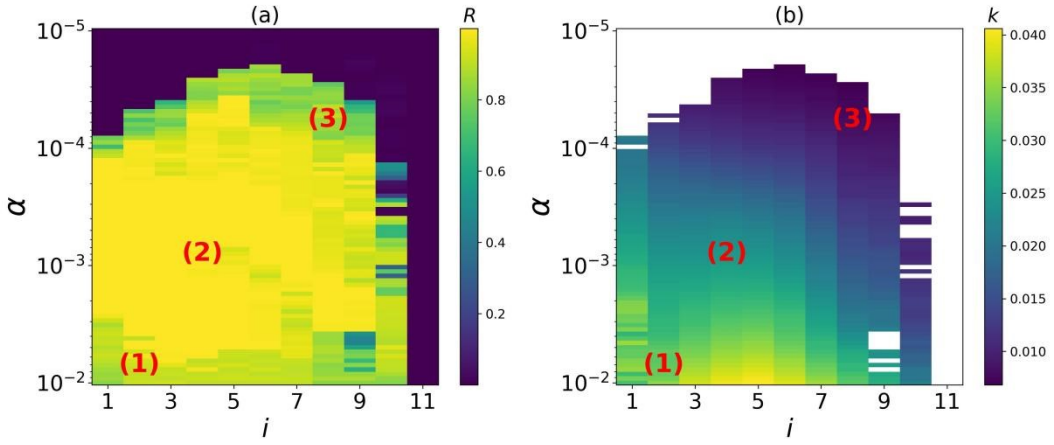


Fig. 8 Statistics of synchronization factor R and electromagnetic induction strength k as a function of the block size and learning rate α under the DLMMS. (For the discrete index $i\epsilon$[1, 11], the associated values satisfies: $(d_i)_{i=1}^{11}$ ={1,2,3,4,5,6,8,10,12,15,20}.) In the statistics, figure b omits the asynchronous magnetic flux density data (shown in white) from the network and displays only the electromagnetic flux density when the network is in a synchronized state. (a) and (b) are broadly divided into three regions. In (b), a slightly smaller value of α can reduce the excitation in the resting-state region caused by low resolution. The effective minimum of k occurs in the deep blue region (3), at which point the network is fully synchronized.

In Fig. 8, we divide the parameter space (d_i, α) into three characteristic regions, as shown in Fig. 8(b): The yellow-green region (1) corresponds to higher α values and

higher resolution. Although the network is capable of achieving global synchronization within this region, the increased magnetic response resulting from the high α values and high resolution leads to a significant increase in the magnetic stimulation intensity required to maintain synchronization. In other words, this region achieves synchronization at the cost of 'high precision and high intensity', and is therefore not the optimal control range. In the light green region (2), whilst a reduction in resolution would normally result in more resting-state regions, appropriately increasing the learning rate α can effectively compensate for this shortcoming—a high α value enhances the responsiveness of adaptive adjustments, thereby making up for the loss of information caused by insufficient spatial resolution. Within this region, the network remains synchronized, and the effects of the reduced resolution are effectively compensated for by optimizing the algorithm parameters, resulting in a significantly lower required magnetic stimulation intensity compared with region (1). The dark blue region (3) corresponds to a resolution equivalent to that of the wave wall; when combined with a learning rate α of approximately 1.0×10^{-4}, this combination of parameters enables the DLMMS method not only to achieve full synchronization of the network, but also to require the lowest magnetic induction intensity of all synchronization regions. In summary, during the DLMMS control process, efficient control of the minimum magnetic flux density can be achieved by adjusting the two parameters: α and resolution.

4. Discussion and conclusion

In this paper, we discuss several methods for eliminating spiral waves in the brain: the use of UMS, AMS, and DLS method to eliminate spiral waves. In these cases, when three different magnetic stimulation conditions were applied to the spiral waves over the same simulation time, our study shows that, after DLS training of the target node, the spiral wave can rapidly achieve indiscriminate electrical synchronization. We compared the DLS method with existing UMS and AMS methods in terms of the minimum required electromagnetic induction strength k, as shown in Fig. 9.

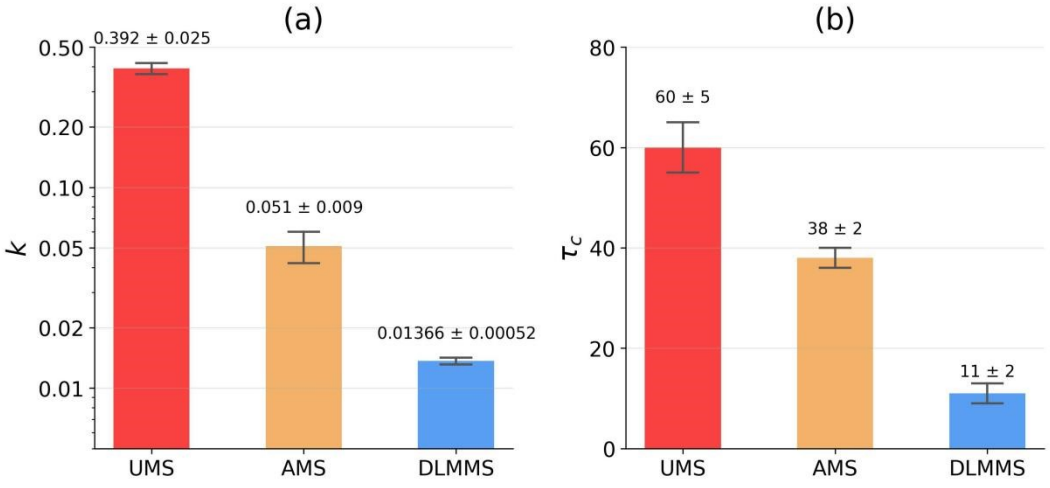


Fig. 9 Comparison of the minimum electromagnetic induction strength required by the three methods, and their convergence times. In the AMS control, the amplitude and frequency are adjusted according to the natural

frequencies of the nodes; in the DLMMS control, adjust the learning rate α and the resolution. (The error bar represents the steady-state synchronization error of the system following multiple independent simulation runs)

As shown in Fig. 9, in the three scenarios described above, the minimum electromagnetic induction strength required for the UMS to eliminate helical waves ranges from 0.367 to 0.417. Although this method is capable of completely and stably eliminating helical waves, it relies on a high and constant magnetic flux density; If the intensity is insufficient, this will induce wave-front fragmentation and turbulent flow, which will in turn exacerbate the chaos within the system. At the same time, as can be seen from Fig. 9(b), the UMS has the longest convergence time, indicating that its dynamic response is the slowest and its real-time control efficiency is relatively low. Encouragingly, the electromagnetic induction strength required to eliminate spiral waves using alternating magnetic stimulation is only 0.042–0.060, which is approximately 11% – 15% of that required for UMS. By utilizing the resonance effect between the frequency of the stimulation and the intrinsic rhythm of the spiral wavefronts, spiral waves can be effectively eliminated and global synchronization achieved within the resonance band. AMS offers advantages such as low force requirements, multiple effective control windows and flexible adjustment; however, its damping effectiveness is highly dependent on frequency resonance and requires precise coordination with amplitude, making parameter matching rather demanding. In terms of convergence performance, AMS significantly shortens the system's transient response and accelerates phase locking between network nodes, resulting in a substantially shorter convergence time compared to UMS.

Compared with the two traditional control methods, UMS and AMS, the advantages of DLMMS lie not only in the significant reduction in electromagnetic induction strength, but also in the system's outstanding adaptive control capabilities. By dynamically learning the electrical activity characteristics of target neurons, the DLS method is able to adapt in real time to the dynamic evolution of the spiral wave head. This avoids the drawbacks of UMS regulation, where the electromagnetic induction strength is fixed and thus unable to cope with dynamic changes in neural electrical activity, and also overcomes the dependence of AMS on resonance frequency. By precisely training nodes within the resolution, DLMMS achieves 'low-intensity, high-precision, high-stability' spiral wave cancellation; the minimum electromagnetic induction intensity required is only 23% – 34% of that of AMS, and less than 4% of that of UMS. Based on a dynamic adaptive learning mechanism, DLMMS significantly optimizes the system's convergence performance: it rapidly locks onto the target node states at the outset of control, thereby substantially shortening the system's transient response; its convergence time is further reduced compared to AMS and is reduced by an order of magnitude compared to UMS. Among the three methods, it demonstrates the best response efficiency and dynamic regulation capability, whilst significantly enhancing the stability of network synchronization.

In this paper, the effectiveness of three methods in eliminating spiral waves is systematically discussed. It clarifies the dual advantages of DLMMS in terms of both

strength and convergence rate, thereby providing strong evidence of the method's effectiveness and superiority in the elimination of low-intensity, high-precision spiral waves. The proposed DLS method offers a novel, effective, and flexible approach to the elimination of spiral waves in excitable media. Although the DLS method performs exceptionally well in eliminating helical waves and thereby achieving electrical synchronization, it still has some limitations. Real cortical tissue has a certain thickness, and the intensity of electromagnetic fields decreases as they pass through tissue of a certain thickness, similar to optical illumination[62] Currently, magnetic stimulation technology[17,18] can be more widely applied to excitable media[53–56], and even extended to magnetically sensitive media[57]. Electromagnetic stimulation has a certain effect on spiral waves in the mammalian neocortex; we can further explore this by combining magnetic field modulation methods[32,37,57]from magnetogenetics[63]. In addition, we can further apply the alternating direction method of multipliers[64,65] to constrain the DLS, thereby further reducing the electromagnetic induction strength required to eliminate the spiral wave. As an exploratory study, this low-intensity magnetic induction strategy is expected to provide a new theoretical perspective and practical guidance for selecting magnetic induction intensities in TMS.

Data availability statement

Hong He and Qianming Ding: Writing − review & editing, Writing − original draft, Visualization, Validation, Methodology, Investigation, Formal analysis, Conceptualization. Weifang Huang and Ying Xie: Validation, Formal analysis. Ya Jia: Writing − review & editing, Supervision, Resources, Project administration, Funding acquisition. Lijian Yang: Writing − review & editing, Supervision, Investigation, Funding acquisition.

Acknowledgment

This work is supported by the National Natural Science Foundation of China under No. 12175080, and also financially supported by self-determined research funds of CCNU from the colleges' basic research and operation of MOE under No. CCNU25JC012 and No. XJ2026007201.

References

[1] Plapp B B, Egolf D A, Bodenschatz E and Pesch W 1998 *Phys. Rev. Lett.* **81** 5334
[2] Sawai S, Thomason P A and Cox E C 2005 *Nature* **433** 323
[3] Kheowan O U, Zykov V S, Rangsiman O and Müller S C 2001 *Phys. Rev. Lett.* **86** 2170
[4] Ouyang Q, Swinney H L and Li G 2000 *Phys. Rev. Lett.* **84** 1047
[5] Winfree A T 1972 *Science* **175** 634
[6] Smolka L B, Marts B and Lin A L 2005 *Phys. Rev. E* **72** 056205
[7] Qu Z, Hu G, Garfinkel A and Weiss J N 2014 *Phys. Rep.* **543** 61
[8] Gray R A, Pertsov A M and Jalife J 1998 *Nature* **392** 75

[9] Zykov V S 2018 *Phil. Trans. R. Soc. A.* **376** 20170379
[10] Pertsov A M, Davidenko J M, Salomonsz R, Baxter W T and Jalife J 1993 *Circ. Res.* **72** 631
[11] Rossi L F, Wykes R C, Kullmann D M and Carandini M 2017 *Nat. Commun.* **8** 217
[12] Smith T M, Esser B D, Antolin N, Carlsson A, Williams R E A, Wessman A, Hanlon T, Fraser H L, Windl W, McComb D W and Mills M J 2016 *Nat. Commun.* **7** 13434
[13] Levy R, Hutchison W D, Lozano A M and Dostrovsky J O 2000 *J. Neurosci.* **20** 7766
[14] Yu H T, Wang J, Du J W, Deng B and Wei X 2015 *Cogn Neurodyn* **9** 93
[15] Huang X Y, Troy W C, Yang Q, Ma H T, Laing C R, Schiff S J and Wu J Y 2004 *J. Neurosci.* **24** 9897
[16] Huang X Y, Xu W F, Liang J M, Takagaki K, Gao X and Wu J Y 2010 *Neuron* **68** 978
[17] Tozzi L, Bertrand C, Hack L M, Lyons T, Olmsted A M, Rajasekharan D, Chen T, Berlow Y A, Yesavage J A, Lim K, Madore M R, Philip N S, Holtzheimer P and Williams L M 2024 *Nat. Mental Health* **2** 987
[18] Hallett M 2000 *Nature* **406** 147
[19] Koponen L M, Nieminen J O and Ilmoniemi R J 2018 *Brain Stimulation* **11** 849
[20] Tian D and Izumi S I 2022 *Front. Neurosci.* **16** 866245
[21] Merton P A and Morton H B 1980 *Nature* **285** 227
[22] Bjekić J, Živanović M, Stanković M, Paunović D, Konstantinović U and Filipović S R 2024 *Front. Hum. Neurosci.* **18** 1468538
[23] Ma K, Vlasov A, Simsek Z B, Zhang J, Li Y, Wang B, Murphy D L K, Choi J Y, Clinton M E, Bukhari-Parlakturk N, Peterchev A V and Goetz S M 2025 *Brain Stimulation* **18** 1918
[24] Li Z, Zhang J, Peterchev A V and Goetz S M 2022 *J. Neural Eng.* **19** 066015
[25] Arai N, Okabe S, Furubayashi T, Terao Y, Yuasa K and Ugawa Y 2005 *Clin. Neurophysiol* **116** 605
[26] Ge M Y, Wang G W and Jia Y 2021 *Sci. China Technol. Sci.* **64** 847
[27] Ma J, Mi L, Zhou P, Xu Y and Hayat T 2017 *Appl. Math. Comput.* **307** 321
[28] Ma J and Tang J 2015 *Sci. China Technol. Sci.* **58** 2038
[29] Hu Y P, Ding Q M, Wu Y and Jia Y 2023 *Chaos, Solitons & Fractals* **175** 113957
[30] Liu Y Q, Hu Y P, Ding Q M, Xie Y and Jia Y 2025 *Chinese Phys. B* **34** 120505
[31] Chua L 1971 *IEEE Trans. Circuit Theory* **18** 507
[32] Huang W F, Wu Y, Ding Q M, Jia Y, Xie Y and Hu Y 2025 *Chaos, Solitons & Fractals* **192** 116001
[33] Xie Y, Ye Z Q, Li X N, Wang X Q and Jia Y 2024 *Cogn Neurodyn* **18** 1989
[34] Xie Y, Huang W F, Jia Y, Ye Z Q and Wu Y 2024 *Physica A* **651** 130037
[35] Lv M, Wang C N, Ren G D, Ma J and Song X L 2016 *Nonlinear Dyn.* **85** 1479
[36] Yang F F, Ma J and Wu F Q 2024 *Chaos, Solitons & Fractals* **187** 115361
[37] Xie Y, Li X N, Wang X Q, Ye Z Q, Hu X Y, Hu Y P and Jia Y 2025 *Nonlinear Dyn.* **113** 12099

[38] Wu F Q, Ma J and Zhang G 2019 *Appl. Math. Comput.* **347** 590
[39] Gao F, Yu X cheng, Deng Y, Yuan F, Wang G Y and Lei T F 2025 *Chinese Phys. B* **34** 120504
[40] Wu F Q, Wang C, Xu Y and Ma J 2016 *Sci. Rep.* **6** 28
[41] Lu L L, Yi M and Liu X 2022 *Sci. China Technol. Sci.* **65** 1661
[42] Ding Q M, Wu Y, Yu D, Li T Y and Jia Y 2023 *Phys. Lett. A* **489** 129154
[43] Rajagopal K, Moroz I, Ramakrishnan B, Karthikeyn A and Duraisamy P 2021 *Nonlinear Dyn.* **104** 4427
[44] Zhang X J, Gu H G and Wu F Q 2019 *Eur. Phys. J. Spec. Top.* **228** 2053
[45] Wu F Q, Hu X K and Ma J 2022 *Appl. Math. Comput.* **432** 127366
[46] Rajagopal K, Jafari S, Karthikeyan A and Srinivasan A 2021 *Chaos* **31** 083115
[47] Wu Y, Ding Q M, Huang W F, Li T Y, Yu D and Jia Y 2024 *Nonlinear Dyn.* **112** 21945
[48] Ding Q M, Wu Y, Huang W F and Jia Y 2025 *Eur. Phys. J. Spec. Top.* **234** 2789
[49] Hu X Y, Wu Y, Ding Q M, Ye Z Q, Xie Y, Jia Y and Zhan X 2025 *Chaos, Solitons & Fractals* **200** 116972
[50] Ye Z Q, Wu Y, Ding Q M, Xie Y and Jia Y 2024 *Phys. Rev. Res* **6** 033071
[51] Wu Y, Ding Q M, Huang W F, Hu X Y, Ye Z Q and Jia Y 2024 *Chaos, Solitons & Fractals* **183** 114896
[52] Huang W F, Wu Y, Ding Q M, Jia Y, Fu Z and Yang L J 2025 *Nonlinear Dyn.* **113** 6671
[53] Ding Q M, Wu Y, Huang W F, Hu Y P, Xie Y and Jia Y 2025 *Nonlinear Dyn.* **113** 10425
[54] Hu Y P, Ding Q M, Wu Y, Yu D, Li T Y and Jia Y 2026 *Chaos, Solitons & Fractals* **204** 117764
[55] Ding Q M, Hu Y P, Li T Y, Xie Y and Jia Y 2026 *Chaos, Solitons & Fractals* **206** 117977
[56] Ding Q M, Hu Y P, Wu Y, Hu X Y, Jia Y and Yang L J 2025 *Chaos, Solitons & Fractals* **191** 115846
[57] Ding Q M, Wu Y, Xie Y, Hu Y P, Huang W F and Jia Y 2025 *Neural Networks* **187** 107379
[58] Rostami Z, Jafari S, Perc M and Slavinec M 2018 *Nonlinear Dyn.* **94** 679
[59] Smith, G. D. 1985 Numerical Solution of Partial Differential Equations: Finite Difference Methods (3rd edn.) (New York: Oxford University Press) pp. 250 - 252
[60] Yu Y G, Hill A P and McCormick D A 2012 *PLoS Comput. Biol.* **8** e1002456
[61] Xu Y, Jia Y, Ge M Y, Lu L L, Yang L J and Zhan X 2018 *Neurocomputing* **283** 196
[62] Bruegmann T, Boyle P M, Vogt C C, Karathanos T V, Arevalo H J, Fleischmann B K, Trayanova N A and Sasse P 2016 *Journal of Clinical Investigation* **126** 3894
[63] Choi S H, Shin J, Park C, Lee J uk, Lee J, Ambo Y, Shin W, Yu R, Kim J Y, Lah J D, Shin D, Kim G, Noh K, Koh W, Lee C J, Lee J H, Kwak M and Cheon J 2024 *Nat. Nanotechnol.* **19** 1333
[64] Liu S, Kong Z M, Huang T, Du Y and Xiang W 2024 *Neural Networks* **173** 106150

[65]Boyd S, Parikh N, Chu E, Peleato B and Eckstein J 2011 *Foundations and Trends in Machine Learning* **3** 1